Chapter 3
TCAD Simulation and Modeling of Ion Implants in Germanium

In this chapter, a TCAD process simulator is used to model dopant implants in germanium. It is then applied to design ion implant steps for a scaled $L_G = 70$ nm germanium pMOSFET technology.

3.1 Introduction

Ion implantation is one of the most widely used processing techniques to introduce impurity atoms into semiconductor materials. Consequently, detailed modeling of ion implantation distributions is a requirement for accurate TCADprocess simulations. The Monte Carlo (MC) simulation method is often used to compute the distribution of implanted ions and the resulting implantation damage. Following years of development, MC simulators have been calibrated to include many combinations of incident ions and substrate atoms (e.g. the SRIM simulator, [161]). However, many only consider amorphous substrate materials. As a result, they cannot capture effects caused by the crystallographic nature of common semiconductor substrates, such as ion channeling. To tackle this issue, MC simulators have been developed and implemented for Si substrates in commercial TCAD software [128] which include the crystallinity of the substrate material, such as crystalTRIM, [116] and TaurusMC, [146]). These simulators lack the required material parameters and calibration to allow detailed modeling of ion implantation into Ge substrates. As such, the first goal of this chapter will be to calibrate one of the MC simulators for ion implants into Ge, including crystallographic effects.

Secondly, although a calibrated Monte Carlo simulator would allow for reliable ion implant simulations, these will inevitably be computationally intensive: statistical noise on ion implant profiles can only be reduced by increasing the number of simulated pseudo-particles, a limitation inherent to the Monte Carlo method. To address this problem, an analytical model will be proposed, describing the ion implant profiles with analytical distribution functions. This approach allows calculation of low-noise ion implant profiles in Ge without the need for time consuming MC simulations.

G. Hellings, K. De Meyer, *High Mobility and Quantum Well Transistors*,
Springer Series in Advanced Microelectronics 42, DOI 10.1007/978-94-007-6340-1_3,

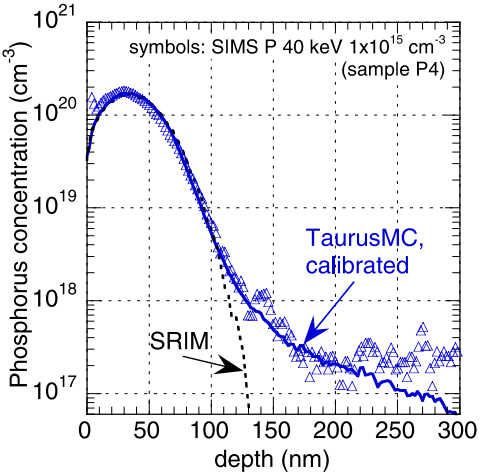

Fig. 3.1 SIMS measurements (*symbols*) and simulated P profiles using the SRIM Monte Carlo simulator [161] and the calibrated TaurusMC

Finally, the calibrated Monte Carlo simulator will be used to design the various ion implant steps required for a scaled $L_G = 70$ nm Ge pFET technology, imitating optimized doping profiles of a 65 nm Si pFET fabrication flow. Fabrication of Ge pFETs with L_G down to 70 nm allows comparison of different implant conditions for the extensions and the halos and benchmarking of these devices versus existing bulk Ge references in literature and the ITRS requirements for the corresponding technology node. Note that only Ge pFETs are considered in this chapter, since essential elements for the fabrication of scaled Ge nFETs need further investigation (e.g. shallow, low-resistive n-type junctions and nFET gate stack passivation).

3.2 Ion Implant into Germanium—Monte Carlo Simulations

The goal of this section is to discuss the calibration of the TaurusMC Monte Carlo TCAD tool for simulating ion implants into Germanium substrates. As mentioned above, accurate simulations of the as-implanted dopant profile in a crystalline solid require the inclusion of ion channeling. One example of this necessity is given in Fig. 3.1, which compares a measured (SIMS) as-implanted phosphorus profile in Ge with two simulated ones. The first profile was obtained using the Stopping Range of Ions in Matter (SRIM) simulator [161]. The main limitation of this simulator is that it considers only structurally isotropic substrates. While this approach yields accurate profiles for implants into amorphous material, it fails to capture important effects in crystalline substrates. Indeed, the crystallinity of the target material introduces an important anisotropy: implanted ions can travel more easily in certain directions, an effect called ion channeling. As such, the SRIM simulator fails to reproduce the deeper part of the implant, where ion-channeling is observed (at depths exceeding 100 nm in Fig. 3.1). The second simulated profile was obtained using the

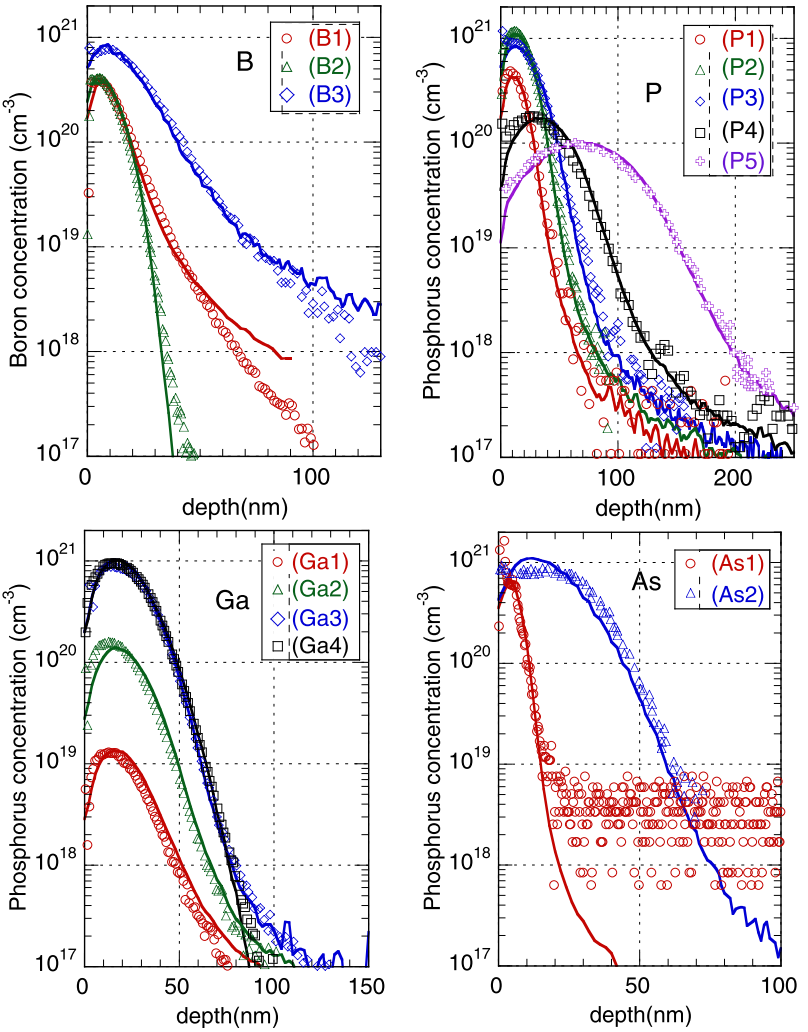

Fig. 3.2 SIMS measurements (*symbols*) and Monte Carlo simulations of I/I profiles into Ge, for various dopants, energies, doses. Sample details are in Table 3.1

calibrated Monte Carlo simulator TaurusMC, which also takes into consideration the crystallinity of the target substrate. Using this simulator, the ion channeling-related portion of the as-implanted profile can be reproduced.

At the beginning of an ion implantation step the crystallographic channels inside the Ge substrate are intact, allowing ions to travel more easily in these directions (ion channeling). However, as displaced lattice atoms clutter these crystallographic channels, this ion channeling process becomes less efficient. This is known as damage de-channeling [128]. Eventually, as even more ions are implanted, these crystallo-

Table 3.1 Overview of the samples used to calibrate the TaurusMC Monte Carlo simulator for I/I into Ge substrates

Sample ID	Reference	Species	Energy (keV)	Dose (cm^{-2})	Tilt-twist (°)	Cap layer (nm)	SIMS (Fig. 2.1)	Amorphous Ge thickness after I/I			
								TEM (nm)	SE (nm)	MC simulated (nm)	delta (%)
B1	Table 2.1 (D11)	B	2.4	8×10^{14}	7–27	none	×	no data			
B2[2]	Table 2.1 (D02)	B	2.4	8×10^{14}	7–27	none	×	no data			
B3	[125]	B	6	3×10^{15}	7–0	10	×	0		0	+0 %
P1		P	12	1×10^{15}	7–0	none	×	no data			
P2	[124]	P	15	3×10^{15}	7–0	none	×	no data			
P3	[125]	P	25	3×10^{15}	7–0	10	×	50		47	−6 %
P4		P	40	1×10^{15}	7–0	none	×	no data			
P5	[137][a]	P	80	1×10^{15}	7–0	none	×	no data			
Ga1	[55]	Ga	40	4×10^{13}	7–0	none	×	no data			
Ga2	[55]	Ga	40	4×10^{14}	7–0	none	×	no data			
Ga3	Section 2.2.1	Ga	40	3×10^{15}	7–0	10	×	58	59	54	−7.7 %
Ga4[b]	Section 2.2.1	Ga	40	3×10^{15}	7–0	none	×	n/a			
Ga5	[55]	Ga	80	3×10^{15}	7–0	none		93		92	−1.1 %
Ga6	[72]	Ga	150	5×10^{13}	7–0	none		108		80	−25.9 %
Ga7	[72]	Ga	150	1×10^{15}	7–0	none		137		138	+0.8 %
Ge1	Section 2.3.1	Ge	20	2×10^{14}	0–0	2			25	20	−20 %
Ge2	Section 2.2.1	Ge	200	1×10^{15}	0–0	none	190		172		−9.5 %
As1	Section 2.3.1	As	5	5×10^{14}	0–0	2	×	8	10	8.5	−5.6 %
As2	[125]	As	50	4×10^{15}	7–0	10	×	50		51.5	+3 %
As3		As	80	5×10^{13}	15–0	11.6			37.3	42	+12.6 %

[a] SIMS depth scale adjusted slightly

[b] Additional ion implants were performed on this sample (prior to the one mentioned)

graphic channels are destroyed completely: the ion bombardment causes complete amorphization of the substrate (to a certain depth), preventing further ion channeling. As a result of this dynamic process, the shape of ion implant profiles into crystalline materials can be heavily dependent on the implanted dose. Low-dose implants will result in a relatively larger channeling tail, while in high-dose implants, most ions will be implanted when the ion channels are already destroyed, yielding a relatively small ion channeling contribution.

A reliable calibration of TaurusMC for implantation of common dopants into crystalline Ge is not generally available. A first set of required parameters contains basic information about the Ge crystal lattice. These physical parameters are generally known and can readily be implemented for any substrate (e.g. atomic mass, mass density, lattice constant, crystal structure, ...). A second set of parameters controls nuclear and electronic stopping of the implanted ions, as they travel through the substrate as well as the damage accumulation in the crystal lattice during the ion bombardment simulation. This second set of parameters is obtained through numerical optimization, aiming for good fitting of the MC simulated profiles to a vast database of experimental SIMS profiles.

In order to calibrate the TaurusMC simulator, the second set of parameters was adjusted, starting from the Si defaults, until good fits were obtained when comparing experimental as-implanted profiles in Ge to their simulated equivalent. The resulting MC simulations and SIMS profiles are plotted in Fig. 3.2(a)–(d) for boron, phosphorus, gallium and arsenic I/I into Ge respectively. Note that the parameters for the I/I of Ga, Ge and As were changed together, as these three elements have a similar atomic mass. The sample processing details are listed in Table 3.1. On some of the samples, a capping layer (mostly SiO_2) was deposited prior to the actual implant (e.g. P3 and B3). Also, some samples received more than one I/I whereby crystallographic damage caused by the first implant can have a profound influence on the distribution of the second implant (e.g. B1 and B2). These effects were included in the MC simulations. Good agreement was obtained between the MC simulations and the SIMS data for P, Ga and As. A modest deviation is observed in the tail portion of the B profiles in Fig. 3.2(a), although the MC simulator is able to reproduce the main features of the profile.

As a fitting to SIMS profiles is still an indirect way to check the damage evolution in the sample during the ion implant and susceptible to measurement noise in the channeling tail, a more direct approach was taken to measure and calibrate the damage evolution in the Ge crystal lattice. For this, the thickness of the amorphous Ge layer created during I/I was measured on various samples using Cross-sectional Transmission Electron Microscopy (TEM) or Spectroscopic Ellipsometry (SE). These measured thicknesses were then compared to the MC simulator's predictions. As can be seen in Table 3.1, the difference between both is generally small, with typical deviations in the range of 0 to 10 %. The adjusted parameters for the TaurusMC simulator are listed in appendix to this chapter and should allow to obtain as-implanted profiles for common dopants in crystallographic Ge with reasonable accuracy.

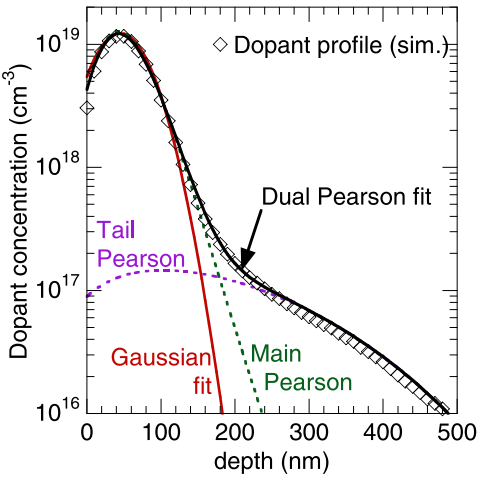

Fig. 3.3 Typical implant profile into a crystalline substrate (*symbols*) and analytical fits using various distributions: Gaussian, Pearson and Dual Pearson

3.3 Ion Implant into Germanium—Analytical Description

3.3.1 Dual Pearson Distribution Functions

Although the calibrated TaurusMC simulator produces good fits to experimental data, it suffers from the fact that the statistical noise inherent to Monte Carlo simulations can only be reduced by increasing the number of simulated pseudo-particles. Combined with the fact that dopant concentration profiles typically span several orders of magnitude, this has a detrimental impact on the required computational power to achieve smooth profiles. This especially limits the applicability of MC simulations when simulating complex 3-dimensional structures.

To address this problem, ion implant profiles have been described using analytical functions such as the Gaussian distribution. A library of calibration tables, containing the parameters of these analytical functions (as a function of species, energy, dose, tilt angle, cap layer thickness etc.) is constructed. This library then allows calculating ion implant profiles with limited computational power using interpolation.

Distribution functions most commonly used for this purpose are the simple Gaussian and the Pearson family of distribution functions of which the Gaussian curve is a member [5]. The tail resulting from ion channeling is often included by use of a second Pearson curve: the sum of the main Pearson and the tail Pearson then represents the entire implantation profile. This approach is illustrated in Fig. 3.3: A typical as-implanted profile from the MC simulator is fitted with a simple Gaussian, a Pearson and a dual Pearson curve. The Gaussian nor the single Pearson can fit the entire profile including the ion-channeling tail. The dual Pearson curve is able to fit the entire profile. Others have constructed different analytical distributions, attempting to capture more of the physics in the analytical model, using e.g. tail functions [135, 137]. Still, the dual Pearson curves are the dominant distribution functions used in commercial TCAD software [128].

The Pearson family of distribution curves contains 12 separately identifiable types and results from solving the differential equation [5]:

$$\frac{df(y)}{dy} = \frac{(x-a)f(y)}{b_0 + b_1 y + b_2 y^2} \tag{3.1}$$

The four parameters of Eq. (3.1) are related to the four moments of the Pearson distribution function: Range R_p, straggle σ_p, skewness γ_p and traditional kurtosis β_p. A dual Pearson curve thus requires 10 parameters: four moments and one normalization factor for each Pearson. Before discussing the analytical model, two remarks are made:

- In this study no restrictions were imposed on the type of Pearson curve used for fitting the ion implant curves. Often specific types of Pearson curves are used to describe ion implant profiles (e.g. the type IV Pearson was proposed by [67]). However as [5] has shown, many other types are also well suited for modeling of ion implant profiles. Therefore, in this work the above-mentioned differential equation (Eq. (3.1)) was solved using the four moments as parameters. The resulting analytic expression is a general solution for a Pearson curve as a function of its four moments: R_p, σ_p, γ_p and β_p.
- Various studies calculate the Pearson moments directly from an ion implant profile using the common statistical definition for the moments. However, Pearson moments calculated directly from the experimental or simulated profiles in this manner will not be sufficiently close to the real moments. The reason for this is that these are inevitably calculated on semi-infinite profiles (covering the range from the boundary presented by the semiconductor surface to a certain maximum analysis depth). Instead, the moments required should be calculated on the whole range of the distribution curve [5, 136]. Therefore, in this study, a numerical least-squares algorithm is used to fit each profile with a dual Pearson curve rather than calculating the moments directly, avoiding this problem.

3.3.2 Analytical Model

Monte Carlo ion implant simulations of P, Ga and As were performed over an energy range of 15–180 keV (P) or 30–360 keV (Ga and As) and for doses ranging from 10^{12} to 10^{16} cm^{-2} at 7° tilt. This range covers the implant conditions generally used in the typical Ge pMOSFETs [33] as well as lower energy conditions which can be of use to future development of both n- and pMOSFETs. Based on these profiles, an analytical model was constructed, allowing to fit the I/I profiles over this entire dose and energy range using dual Pearson curves. This model and its parameters are contained in Table 3.2. Most of the Pearson moments were fitted using a second order polynomial and can be considered a function of energy only. For the main Pearson curve, only the skewness is a function of both implant energy and dose, an effect linked to ion channeling. For the tail Pearson, the skewness and kurtosis

Table 3.2 Overview of the parameterized analytical model for ion implants into crystalline substrate

	Main Pearson	Tail Pearson
R_p (nm)	$p_0 + p_1 E + p_2 E^2$	$p_{14} R_p$
σ_p (nm)	$p_3 + p_4 E + p_5 E^2$	$p_{15} \sigma_p$
γ_p (–)	$p_6 + p_7 E + p_8 E^2 + p_9 (1 - (\frac{D}{D+p_{10}})^3)^3$	0
β_p (–)	$p_{11} + p_{12} E + p_{13} E^2$	3.36
dose (cm^{-2})	$D - D_{tail}$	$\begin{cases} D_{tail} = (1/d_a + 1/d_b)^{-1} \\ d_a = p_{16} D \\ d_b = (\frac{D}{10^{13}})^{p_{17}} p_{18} \end{cases}$

were fixed for numerical stability. Finally, the fraction of the implanted dose that is attributed to the tail Pearson (channeling dose) is modeled considering two regimes:

- For low dose implants, the fraction of ions that are contained in the channeling tail is constant as a function of the implanted dose. This can be explained by considering that for low implanted doses, the crystallographic channels inside the substrate remain intact during the entire I/I step. As such, every implanted ion has an equal chance of ending up in the channeling tail (d_a in Table 3.2, low-dose limit in Fig. 3.4).
- For high-dose implants, the absolute number of ions that are contained in the channeling tail is rather constant. This can be explained by considering that for high implanted doses, the crystallographic channels get destroyed at one point during the I/I. Any ions implanted beyond this point will not end up in the channeling tail, giving rise to an almost constant number of ions in the channeling tail. (d_b in Table 3.2, high-dose limit in Fig. 3.4).
- Finally, these two regimes are combined in final formula for the channeling dose (D_{tail} in Table 3.2) with a smooth transition.

The parameters of the resulting analytical model were obtained using a numerical optimization algorithm minimizing the total fitting error between the Monte Carlo simulated I/I profiles and the analytical profiles for P, As and Ga. The resulting values can be found in Table 3.5 in Appendix A.2. Boron was omitted here as a species, since the fit between the MC simulations and measured SIMS data was of lesser quality than for the other dopants. Note that the parameters p_0–p_{18} should purely be considered as empirical fitting parameters.

3.3.3 Practical Applications

A first practical application of this analytical model is obviously that it allows to quickly predict an ion implant profile. As an example of this, Fig. 3.5 contains three measured SIMS profiles (various Ga and P implants), the simulated profiles using

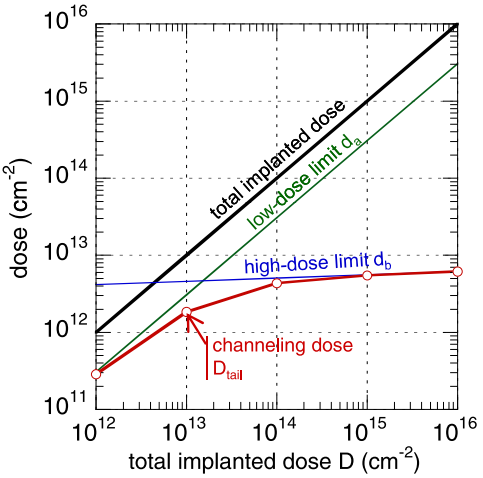

Fig. 3.4 Channeling dose dependence as a function of total implanted dose for phosphorus implants into crystalline germanium showing the combination of the low-dose limit d_a (channeling dose proportional to total implanted dose and the high-dose limit d_b (channeling dose nearly constant)

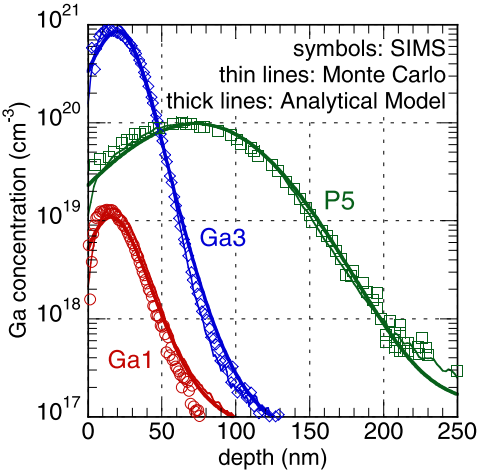

Fig. 3.5 Doping profiles of Ga and P in Ge as obtained from SIMS measurements (*symbols*), the calibrated Monte Carlo simulator (*thin lines*) and the analytical model (*thick lines*)

the calibrated MC simulator and the calculated profiles using the analytical model. For each of these conditions, the difference between all three are rather small. Note that the energy of these conditions was not used to obtain the model parameters. The advantage of using the analytical model becomes clear when comparing the time required to obtain such 1-dimensional profiles. While the MC simulator took 6 minutes (P5 profile), the analytical profile was calculated in less than 1 second. Additionally, the MC simulated profiles have clearly visible statistical noise (e.g. in the 10^{17} cm^{-3} range for the P5 profile). This performance gap increases even more when comparing simulations in 2D or 3D (e.g. process simulations of a typical transistor).

A second practical application is that this analytical model can be used to construct implantation tables for I/I of common dopants in germanium. Many modern

process simulators use such calibration tables containing (dual) Pearson moments as a function of energy, dose, tilt angle, and other parameters. With the analytical model, such tables can be constructed containing many profiles (i.e. many energy/dose combinations) starting from a limited set of MC simulations.

3.3.4 Conclusions

In the previous sections, the Taurus Monte Carlo simulator was calibrated for ion implants of boron, phosphorus, gallium, germanium and arsenic into Germanium based on experimental SIMS profiles. Additionally, the thickness of the amorphous layer induced by the I/I was used as a second calibration using TEM and SE measurements. As such, accurate simulations of as-implanted dopant profiles can now be performed, taking into account such crystal lattice effects as ion-channeling in Germanium. An analytical model was proposed based on the description of as-implanted dopant profiles using dual Pearson distribution curves (P, Ga, As). This model spans an energy/dose range which should cover most of the I/I conditions relevant for short channel Ge p- and nMOSFET development. This analytical description allows calculation of low-noise I/I profiles in Ge without the need for time consuming MC simulations.

3.4 Application to a 70 nm Bulk Ge pFET Technology

In this section, high performance Ge pMOSFETs will be presented with physical gate lengths down to 70 nm. The various implant steps were designed using the calibrated MC implant simulator to mimic the doping profiles in an optimized 65 nm Si pFET fabrication flow. On top of this, different extension and halo implant conditions are compared. Finally, the 70 nm Ge pFET device is benchmarked against existing bulk Ge references in literature and against ITRS requirements for the corresponding technology node.

3.4.1 Imitating Si Doping Profiles—'Simitation'

$L_G = 70$ nm Ge pFETs with good short channel behavior require careful optimization of the source/drain doping profiles and the halo implants. A good starting point for this engineering exercise can be found by imitating the doping profiles in an optimized $L_G = 65$ nm pFET silicon technology. The calibrated Monte Carlo ion implant simulator is obviously a very useful tool to obtain these Ge I/I conditions. Therefore, combining 1-dimensional SIMS analysis with the MC simulator in the following paragraphs, we will try to match the $L_G = 65$ nm Si doping profiles with

Ge conditions. Note that this approach will only provide a starting point, not a complete set of optimized ion implant conditions for Ge for two reasons. Firstly, matching the chemical dopant concentration observed in Si with as-implanted dopant profiles in Ge does not—in general—yield identical charge carrier profiles. However at the dopant concentrations generally found in scaled pFETs (below 1×10^{19} cm^{-3} for n-type dopants), diffusion of dopants in Ge is rather small, as discussed in Chap. 2. As a result, the as-implanted dopant profiles in Ge will be a good approximation of the final dopant distribution (after the activation anneal). Secondly, the specific material properties of Ge will most likely require different dopant distributions for optimal pFET performance. For example, Ge's smaller band gap may require a smaller electric field in specific regions to reduce junction leakage. Keeping these limitations in mind, the different I/I processing steps are discussed (detailed conditions are in Table 3.3):

- *Well doping*—The higher atomic mass of Ge results in broader as-implanted profiles, compared to Si, as mentioned before. As a result, when attempting to obtain the same deep well profile as in Si, the broader P profile results in a too high channel doping. To avoid this, the deep well dose was lowered. In combination with matching conditions for the APT (Anti Punch Through) and VTA (V_T Adjust) well implants, the resulting P profile in Ge is quite close to its counterpart in Si, considering that the actual device is fabricated in the top 100 nm of the wafer (Fig. 3.6(a)). While using As for the deep well implants would allow matching the Si deep well profile, its higher atomic mass would cause the top 500 nm Ge to be amorphized as a result of the I/I at the required conditions, which is obviously not desired.
- *Halo doping*—The Si halo reaches a maximum As concentration of about 1×10^{19} cm^{-3} at a depth of 20–30 nm. The P halo implants (30–40–60 keV) which were successfully used in the $L_G = 125$ nm Ge pFETs [105] are all broader than the Si target halo profile, while not reaching the same peak concentration. For this reason an 80 keV As halo was chosen, matching the Si target profile in the first 20–30 nm and reaching the same peak concentration. As the extension depth is about 20–30 nm for a 65 nm technology, the slightly deeper tail of this halo implant is expected to have limited or no influence on the short channel behavior, although junction leakage might increase.
- *Extension doping*—While in the Si pFET, the as-implanted B extension profile is very shallow (the B concentration drops below 1×10^{19} cm^{-3} at a depth of only 12 nm), the 1050 °C spike anneal causes significant in-diffusion. Consequently, the as-implanted profile is not relevant for this exercise. In Ge, B is largely diffusionless up to 700 °C (see Sect. 2.2.2). Considering even lower 550 °C Ge junction anneal, the as-implanted B profiles in Ge can be considered a good approximation of the final B distribution. As shown in Fig. 3.6(c), a 2 keV, 8×10^{14} cm^{-2} B implant into Ge yields the same junction depth as its Si equivalent (measured using SIMS to account for the aforementioned B diffusion during the spike anneal). Note that the Ge extensions have a higher B concentration near the surface, which will give rise to a lower pFET series resistance assuming this extra B is electrically active.

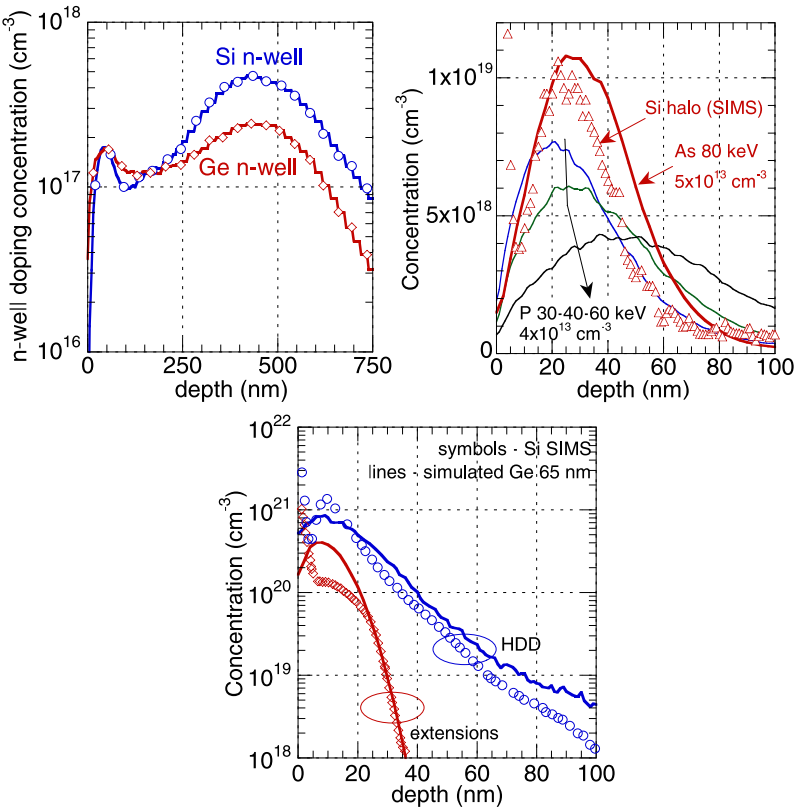

Fig. 3.6 Simulated or measured ion implant conditions for a Si $L_G = 65$ nm pFET flow and the matched Ge implant conditions (see also Table 3.3)

- *HDD doping*—Finally a 6 keV, 3×10^{15} cm^{-2} B implant is shown to yield a similar profile as its Si HDD equivalent. However, a preceding Ge preamorphization step is required in order to improve the electrical B activation and prevent an excessive ion-channeling tail (this was included in the MC simulation in Fig. 3.6(c).

3.4.2 Experimental Details

Ge pMOSFET devices were fabricated on 200 mm diameter, (100)-oriented Si wafers on which a relaxed Ge layer was grown to a thickness of 1.5 µm. The wafers were first annealed at 850 °C for 3 min to reduce the threading dislocation density to approx. 2×10^7 cm^{-2} [16]. The basic Si-compatible process flow is described in [33]. A phosphorus channel doping of about 3×10^{17} cm^{-3} was implanted, followed by deposited SiO_2 isolation. The Ge surface was passivated by a thin, partially oxidized epitaxial Si layer, as described in [16, 32], and capped with 4 nm HfO_2, after

Table 3.3 Ion implant conditions for the Si $L_G = 65$ nm pFET flow and matched Ge implant conditions

Process step	Ge 65 nm implants
n-well	P 540 keV, 1×10^{13} cm^{-2}, 7°
APT	P 190 keV, 1×10^{12} cm^{-2}, 7°
VTA	As 175 keV, 1×10^{12} cm^{-2}, 7°
Well anneal gate module	300 sec, 600 °C, N_2
Halo	As 80 keV, 5×10^{13} cm^{-2}, 15°
Extensions spacer module	B 2 keV, 8×10^{14} cm^{-2}, 0°
HDD	Ge 35 keV, 1×10^{15} cm^{-2}, 0°
	B 6 keV, 3×10^{15} cm^{-2}, 0°
Junction anneal	5 min RTA, 550 °C, N_2

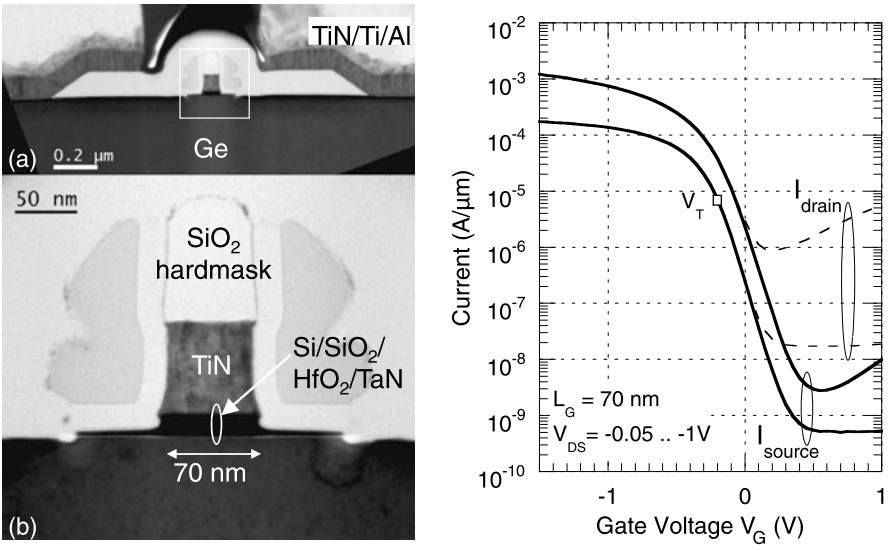

Fig. 3.7 Cross-sectional TEM image of a $L_G = 70$ nm Ge pMOSFET (**a**)–(**b**) and I_S–V_G/I_D–V_G characteristics for the 70 nm Ge pMOSFET with 'B only' extensions (**c**)

which a TaN/TiN metal gate is deposited. On the reference process, arsenic halos are implanted (80 keV, 5×10^{13} cm^{-2}, 15° tilt), followed by BF_2 extensions (11 keV, 8×10^{14} cm^{-2}). Spacer definition and HDD implants are followed by NiGe S/D formation (5 nm Ni deposited, 2-step RTP flow, [16]) and TiN/Ti/Al/TiN back-end processing [15].

Besides the reference flow just described (Process Of Reference—POR), devices were also fabricated with different implant conditions for the halo and extension doping. A 'shallow halo' was implanted using As, 60 keV, 4.5×10^{13} cm^{-2}, 15° tilt, a 'deep halo' was implanted using As, 100 keV, 5.5×10^{13} cm^{-2}, 15° tilt. The doses in all three conditions were changed slightly to maintain the same As peak

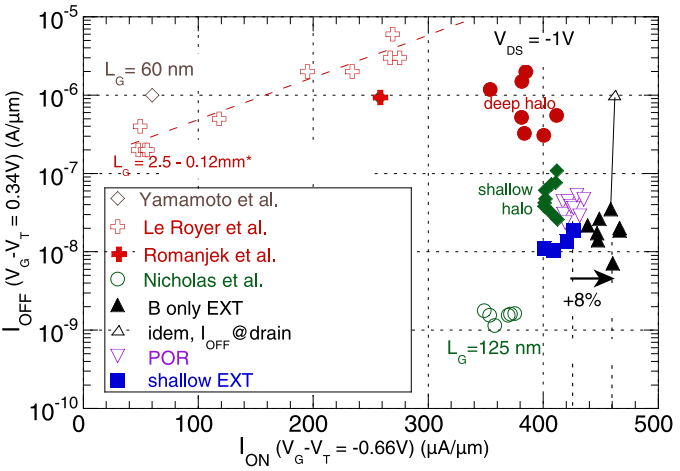

Fig. 3.8 I_{ON}–I_{OFF} relationship for the Ge pMOSFETs at $V_{DD} = 1$ V, evaluated at the source (various splits) and comparison with literature. A boost in I_{ON} is observed using 'B only' extensions

concentrations on the as-implanted profile. A 'shallow extension' was implanted by lowering the BF_2 implant energy to 9 keV while a 'B only' extension was fabricated using a B implant at 2.42 keV. The as-implanted profile B of the 'B only' condition is closely matching the 11 keV BF_2 POR extension I/I, while the 'shallow extension' condition using BF_2 matches a 2 keV B implant.

Note that the ion implant conditions used in the following sections are somewhat of a compromise between the existing Ge process flow, designed for L_G down to 125 nm, [105] and the 'Simitation' conditions discussed above. Still, essential elements such as the As halo, B extensions instead of BF_2 and a shallow extension split were included and will be discussed in detail.

Figure 3.7(a)–(b) shows a cross-sectional TEM image of the Ge pMOS with a gate length of 70 nm. The small voids next to the spacers were formed during the NiGe process module. While the exact reason is still under investigation, they may have an negative impact on the devices' electrical characterization.

3.4.3 Electrical Characterization

3.4.3.1 General Analysis

Figure 3.7(c) shows the I_S–V_G and I_D–V_G characteristics for the 70 nm Ge pMOSFET with 'B only' extensions for a V_{DS} of −50 mV and −1 V. A saturation drive current (I_{ON}) of 467 µA/µm is obtained for $V_G - V_{T,sat} = -0.66$ V and $V_{DS} = -1$ V, with an OFF-state current (I_{OFF}) of 2×10^{-8} A/µm at $V_G - V_{T,sat} = 0.34$ V, evaluated at the source. While I_{OFF} is conventionally measured at the drain to

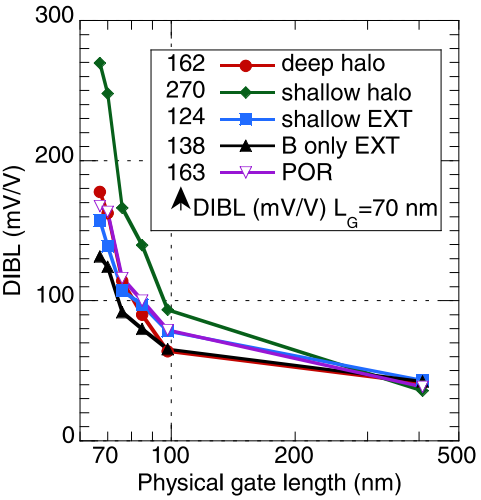

Fig. 3.9 DIBL vs. L_G for the Ge pMOSFET devices (various splits)

include drain-to-bulk diode leakage, Ge, with its smaller band gap suffers from higher diode leakage at the drain/well junction than equivalent Si devices [38] due to increased trap-assisted-tunneling mechanisms. Unfortunately the test devices discussed in this section have a rather large drain area of 148 μm^2, several orders of magnitude larger than those used for deep submicrometer devices. Measurements on devices with different drain areas have shown that this drain-to-bulk junction leakage varies with area. As such, evaluating I_{OFF} at the drain would result in an overestimation for realistic device dimensions. Therefore, I_{OFF} is measured at the source rather than estimating its value for small active areas. Nevertheless, drain-side I_{OFF} will be included in the further benchmarking of these Ge pFETs. The issue of drain-to-bulk leakage for Ge pMOSFETs will be discussed in more detail in Sect. 5.2.1.

The effective oxide thickness (*EOT*) of the gate stack is 1.4 nm. The gate leakage is less than 10^{-3} A/cm^2 (measured at $V_G = V_T - 0.6$ V). The V_T is about 0 V for long-channel devices and -200 mV for the 70 nm pFET (on target for high performance logic applications). This lower V_T is the result of the halo implants, which dominate for short devices (pFET V_T roll-up). Long channel V_T can be lowered by increasing the well doping, which will have limited or no impact on short channel devices where the halo doping dominates. Halo and well doping can thus be optimized together to obtain the desired flat V_T behavior as a function of gate length. Figure 3.8(a) shows the I_{ON}–I_{OFF} relationship for Ge pMOSFETs evaluated at the source. To compensate for the off-target V_T the V_G swing is shifted such that I_{ON} and I_{OFF} are measured at $V_G - V_{T,sat} = -0.66$ V and $V_G - V_{T,sat} = +0.34$ V respectively, as suggested by [19]. Available short channel Ge pFETs were added for comparison, including 60 nm devices with full NiGe source/drains [159] and devices fabricated on Germanium-On-Insulator substrates (GOI) [92, 121].

3.4.3.2 Extension Optimization

Comparing the different extensions implant conditions, two effects can be observed. First, reducing the BF_2 extension energy from 11 to 9 keV results in a decrease of I_{OFF} (Fig. 3.8) and *DIBL* from 163 to 124 mV/V (Fig. 3.9). This improved short channel behavior is of course linked to the smaller implant energy, which results in shallower extensions. In addition, the 'B only' extensions result in an 8 % I_{ON} boost, as compared to their BF_2 counterparts. At the same time a reduction in short channel effects is also observed (*DIBL* = 138 mV/V). Consequently, the I_{ON} boost cannot be caused by a reduced electrical gate length, as this would result in degraded short channel behavior. To pinpoint the cause, the devices' series resistance R_{EXT} was extracted using the method described in [140]. It was found that using the 'B only' extensions reduced R_{EXT} from 145 to 100 Ω µm. Using a linear approximation, such a decrease in R_{EXT} would explain a 5 % I_{ON} boost, which is quite close to the observed value.

Linking these pFET device results to the blanket boron shallow junction experiments performed in Sect. 2.2.2 confirms that the co-implantation of boron with fluor in Ge degrades junction properties. In the junction experiment, R_{sh} increased from 153 to 425 Ω/sq. Considering an extension length of 70 nm on either side of the gate, the total source and drain extension resistance would be 68 and 24 Ω µm for the POR and 'B only' extensions respectively. The difference of 43 Ω µm between these two accounts almost fully for the observed improvement in pFET series resistance R_{EXT}. As such, it is clear that the co-implantation of B with F, although necessary in Si technology to reduce B diffusion, degrades Ge pFET performance and should be avoided if possible to obtain higher I_{ON}.

3.4.3.3 Halo Optimization

Comparing the different halo implant conditions (POR, shallow halo, deep halo) a degradation is observed for both deviations from the POR condition in Fig. 3.8. Relative to the POR condition, the 'deep halo' condition significantly increases drain-to-bulk junction leakage, leading to 1–2 orders of magnitude higher I_{OFF}, while *DIBL* is almost unchanged for the $L_G = 70$ nm pFET. This clearly signifies that this halo implant condition results in a too deep halo, increasing the electric field and, as a result, the junction leakage while doing little to further improve short channel control. For the shallower halo, *DIBL* is severely degraded, leading to a mild increase in I_{OFF} in combination with a small I_{ON} penalty, indicating a too shallow halo placement.

3.4.4 Benchmarking

An important question for Ge is whether its high bulk mobility translates into high performing short-channel devices, as compared to Si. For aggressively scaled devices, carrier velocity saturation can be a key limiter for device performance. However, [109] has shown that hole velocity is higher in Ge compared to Si (maintaining similar parasitic effects). Here, we will compare the $L_G = 70$ nm Ge pFETs

Table 3.4 Comparison of key parameters for a $L_G = 70$ nm Ge pMOSFET and the ITRS specifications for the corresponding technology node (physical $L_G = 65$ nm) showing a 50 % higher I_{ON} for the Ge pFET

	ITRS 2002, [73] $L_G = 65$ nm	Ge pFET $L_G = 70$ nm
Physical gate length L_G (nm)	65	70
Equivalent oxide thickness EOT (nm)	1.3–1.6	1.4
Power supply voltage V_{DD} (V)	1.2	1.2
Saturation drive current I_{ON} (μA/μm)	400–450	622
saturation source off-state current I_{OFF} (A/μm)	2.4×10^{-8}	2.1×10^{-8}
Saturation drain[a] I_{OFF} (A/μm)		9×10^{-7}
Saturation I_{ON} at $V_{DD} = 0.95$ V (μA/μm)		432

[a]Overestimation for realistic device dimensions due to large drain area of 148 μm^2

with 'B only' extensions with strained Si, using the benchmarks proposed in [19]. Figure 3.10(a) shows the intrinsic gate delay as a function of the I_{ON}–I_{OFF} ratio for Ge pFETs (our devices, [105]) and a strained Si reference with similar EOT ($I_{ON} = 422$ μA/μm, [154]). The 70-nm Ge device offers a significant improvement over the 80-nm strained Si device for any I_{ON}–I_{OFF} ratio up to 4×10^4. A second metric is the intrinsic gate delay as a function of L_G (Fig. 3.10(b)). Also here, a certain benefit of Ge with respect to strained Si can be observed down to $L_G = 70$ nm. The third metric proposed in [19] is the linear subthreshold slope as a function of L_G. For our Ge devices, this quantity is rather constant at 120 mV/V. This high constant value indicates that further optimization of the gate stack is required before any conclusions can be drawn regarding the short channel control using this metric. The fourth benchmark (energy delay product as a function of L_G) is not discussed, as it will show the same as the second benchmark since we have benchmarked all devices at the same supply voltage and at similar EOT.

Comparing our Ge pMOS with the ITRS specifications for $L_G = 65$ nm (130 nm node, [73]) demonstrates the performance advantage. Table 3.4 summarizes the data and benchmarking conditions of this comparison. The Ge device exceeds the ITRS I_{ON} requirements by almost 50 %, maintaining a similar I_{OFF}, as measured at the source. A second comparison shows that the Ge pMOSFET can reach this ITRS specification ($I_{ON} = 432$ μA/μm) at a reduced V_{DD} of 0.95 V, yielding a 40 % reduction in active power dissipation, thanks to the V_{DD}-scaling ($P = fCV_{DD}^2$). This performance improvement is obtained despite the still slightly larger physical gate L_G for the Ge devices.

The significance of this benchmarking exercise is that is indicates that the higher mobility of Ge indeed translates into a higher drive current I_{ON}, even for sub-100 nm devices. Still, as more techniques arise to further strain Si devices, Ge FETs will, in turn, also require strain-boosters to keep outperforming (strained) Si: with a channel stress in excess of 1 GPa, the ballistic hole velocity in Ge devices would be higher than the limit in strained silicon based on simulations, [3]. A second is-

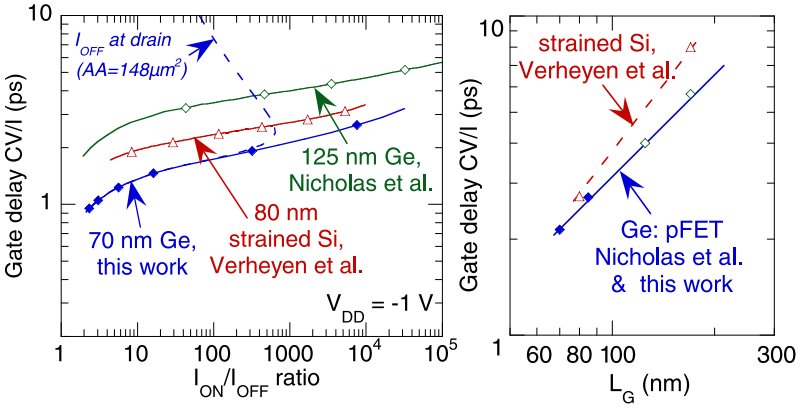

Fig. 3.10 Intrinsic gate delay as a function of I_{ON}–I_{OFF} ratio (**a**) and of gate length (**b**) for Ge (this work and [105]) and strained Si pMOSFETs [154]—Benchmarks from [19]

sue which needs to be investigated is the drain-to-bulk leakage in scaled devices. Addressing this issue, a scalability study of bulk Ge devices will be discussed in Sect. 5.2.1.

3.4.5 Conclusions

In this section, high performance Ge pMOSFETs were presented with physical gate lengths down to 70 nm. The ion implant process steps were designed to provide good short channel control in these devices by mimicking the doping profiles of an optimized 65 nm Si pFET technology using the calibrated Monte Carlo ion implant simulator. Different extension and halo implant conditions were compared. Firstly, the 80 keV As halo implant was shown to be optimal in terms of implant depth, with both shallower and deeper halo implants causing reduced short channel control and excessive junction leakage respectively. Secondly, reducing the extension depth and changing the implant species from BF_2 to atomic B resulted both in better short channel control and decreased pFET series resistance respectively. Benchmarking shows the potential of Ge to outperform (strained) Si as a pFET channel material well into the sub-100 L_G regime. The 70 nm devices outperform the ITRS requirements for I_{ON} for the corresponding node by about 50 %, maintaining a similar I_{OFF} measured at the source. In addition, the Ge device matched these ITRS specifications at a reduced V_{DD} of 0.95 V, resulting in a 40 % reduction in active power dissipation, owing to V_{DD} scaling.

3.5 Summary and Conclusions

In this chapter, a Monte Carlo simulator was calibrated to enable TCAD process simulations of ion implants into germanium substrates. Simulated as-implanted concentration profiles for B, P, Ga and As showed good agreement with measured data,

obtained using Secondary-Ion Mass Spectroscopy measurements. Additionally, the thickness of the amorphous Ge layer created during the I/I as measured using Cross-sectional Transmission Electron Microscopy (TEM) or Spectroscopic Ellipsometry (SE), was shown to agree with the simulator's predictions, with typical deviations in the range of 0 to 10 %. Consequently, the calibrated MC simulator allows reliable simulations of as-implanted profiles and amorphization depths for common dopants in crystalline Ge.

In a second section, an analytical model was proposed based on the description of as-implanted dopant profiles (P, Ga, As) with dual Pearson distribution curves. This model allows a fast, straightforward way to obtain low-noise I/I profiles for these dopants in Ge and covers an energy-dose range comprising many conditions relevant for short channel Ge p- and nMOSFET development.

Then, using the calibrated Monte Carlo simulator, the ion implant steps required for a scaled $L_G = 70$ nm Ge pFET technology were designed, based on the optimized I/I profiles for a 65 nm Si pFET fabrication flow. Using many of those I/I conditions, high performance Ge pMOSFETs were fabricated with physical gate lengths down to 70 nm, allowing the comparison of different conditions for the extension and halo ion implants. An 80 keV (5×10^{13} cm^{-2}, 15° tilt) As halo implant was shown to be optimal in terms of implant depth for this technology. pFET series resistance was shown to decrease by changing the extension implant species from BF_2 to atomic boron, thus confirming the results obtained in blanket junction experiments (Chap. 2).

Finally, a benchmarking exercise showed the potential of germanium to outperform strained-silicon as a channel material well into the sub-100 L_G regime: 70 nm devices outperform the ITRS requirements for I_{ON} by about 50 %, maintaining a similar I_{OFF}, measured at the source. In addition, the Ge pFETs matched ITRS specifications with a 40 % reduction in active power dissipation, owing to V_{DD} scaling.

Appendix

A.1 Calibrated Parameters for TaurusMC

This appendix contains the calibrated parameters for the Taurus Monte Carlo Ion Implant simulator (using sprocess syntax, [128]).

```
PHYSICAL MODELS FOR GERMANIUM
pdbSetDouble ImplantData Germanium AtomicMass 72.61
pdbSetDouble ImplantData Germanium AtomicNumber 32
pdbSetDouble Germanium LatticeConstant 5.64613
pdbSetDouble Germanium LatticeDensity 4.41e22
pdbSetDouble Germanium AmorpGamma 1.0
pdbSetDouble Germanium AmorpDensity 1.1e22
pdbSetDouble Germanium AmorpThreshold 1.1e22
pdbSetDouble Germanium LatticeSpacing [expr pow(1/4.41e22,1.0/3.0)]
```

```
pdbSetString Germanium LatticeType Zincblende
pdbSetDouble Germanium MassDensity 5.35
pdbSetBoolean Germanium Amorphous 0
pdbSetString Germanium LatticeAtom COMPOSITION
pdbSetString Germanium Composition Component0 Name Germanium
pdbSetDouble Germanium Composition Component0 StWeight 1
pdbSetDouble Germanium CompoundNumber 1
pdbSetDouble Germanium DebyeTemperature 519
pdbSetBoolean Germanium ElectronicStoppingLocal 1
pdbSetDouble Germanium SurfaceDisorder 5e-4



NUMERICAL PARAMETERS FOR TaurusMC (please consult manual)
pdbSet MCImplant TrajectoryReplication 0
pdbSet MCImplant TrajectorySplitting 1
pdbSetDouble Germanium Phosphorus MaxSplits 8.0
pdbSetDouble Germanium Phosphorus MaxSplitsPerElement 1.0
pdbSetDouble Germanium Boron MaxSplits 8.0
pdbSetDouble Germanium Boron MaxSplitsPerElement 1.0
pdbSetDouble Germanium Arsenic MaxSplits 8.0
pdbSetDouble Germanium Arsenic MaxSplitsPerElement 1.0


Monte Carlo Implant paramerters implanted species (TaurusMC)
pdbSetDouble Germanium Phosphorus amor.par 1.0
pdbSetDouble Germanium Phosphorus casc.amo 1.0
pdbSetDouble Germanium Phosphorus disp.thr 15
pdbSetDouble Germanium Phosphorus casc.dis 15
pdbSetDouble Germanium Phosphorus surv.rat 0.75
pdbSetDouble Germanium Phosphorus casc.sur 0.75
pdbSetDouble Germanium Phosphorus MCVFactor 1.0
pdbSetDouble Germanium Phosphorus MCDFactor 1.0
pdbSetDouble Germanium Phosphorus MCIFactor 1.0

pdbSetDouble Germanium Boron amor.par 1.0
pdbSetDouble Germanium Boron casc.amo 1.0
pdbSetDouble Germanium Boron disp.thr 15
pdbSetDouble Germanium Boron casc.dis 15
pdbSetDouble Germanium Boron surv.rat 0.225
pdbSetDouble Germanium Boron casc.sur 0.225
pdbSetDouble Germanium Boron MCVFactor 1.0
pdbSetDouble Germanium Boron MCDFactor 1.0
pdbSetDouble Germanium Boron MCIFactor 1.0

pdbSetDouble Germanium Boron casc.sat 0.02
pdbSetDouble Germanium Boron sat.par 0.02
THESE PARAMETERS makes B only partially amorphizing in Germanium,
damage saturates when 2% of lattice atoms have been
displaced. This number is based on LIMITED SIMS data
and should be considered an estimate.
pdbSetDouble Germanium Arsenic amor.par 1.0
pdbSetDouble Germanium Arsenic casc.amo 1.0
```

```
pdbSetDouble Germanium Arsenic disp.thr 15
pdbSetDouble Germanium Arsenic casc.dis 15
pdbSetDouble Germanium Arsenic surv.rat 0.9
pdbSetDouble Germanium Arsenic casc.sur 0.9
pdbSetDouble Germanium Arsenic MCVFactor 1.0
pdbSetDouble Germanium Arsenic MCDFactor 1.0
pdbSetDouble Germanium Arsenic MCIFactor 1.0
```

A.2 Model Parameters: Ion Implants into Crystalline Ge

Table 3.5 Model parameters for the analytical ion implant modeling (see Sect. 3.3.2)

Species	p_0	p_1	p_2	p_3	p_4
P	-1.00×10^{-2}	8.58×10^{-1}	-1.00×10^{-1}	6.45	5.14×10^{-1}
Ga	-1.00×10^{-2}	4.23×10^{-1}	-1.00×10^{-1}	7.42	2.40×10^{-1}
As	-1.00×10^{-2}	4.03×10^{-1}	-1.00×10^{-1}	7.53	2.11×10^{-1}
Species	p_5	p_6	p_7	p_8	p_9
P	-6.72×10^{-4}	-4.01×10^{-1}	1.87×10^{-3}	-1.34×10^{-5}	1.01
Ga	-1.77×10^{-4}	-8.74×10^{-1}	3.12×10^{-3}	-5.74×10^{-6}	1.23
As	-1.25×10^{-4}	-7.44×10^{-1}	2.95×10^{-3}	-6.40×10^{-6}	1.27
Species	p_{10}	p_{11}	p_{12}	p_{13}	p_{14}
P	1.79×10^{14}	4.90	-2.17×10^{-2}	7.94×10^{-5}	2.71
Ga	9.04×10^{13}	7.78	-2.03×10^{-2}	2.62×10^{-5}	2.52
As	8.99×10^{13}	7.01	-1.84×10^{-2}	2.79×10^{-5}	2.64
Species	p_{15}	p_{16}	p_{17}	p_{18}	
P	4.23	3.06×10^{-1}	4.29×10^{-2}	4.58×10^{12}	
Ga	5.47	3.25×10^{-1}	-1.00×10^{-4}	2.46×10^{12}	
As	5.70	3.17×10^{-1}	-1.00×10^{-4}	2.29×10^{12}	